PERFORMANCE STUDY OF A TIME-OF-FLIGHT METHOD USED FOR COSMIC RAY DETECTION

Alİ Yilmaz

Department of Electrical and Electronics Engineering, Giresun University
28200 Giresun, Turkey

(Received March 17, 2019; accepted June 14, 2019)

Time-of-Flight methods have been rapidly developed and recently used in many experiments for determination of particle direction, identification of particles and energy resolutions. This paper describes a method of time-mark determination on the reconstruction algorithm, based on the sampled signal, used for time-of-flight measurements. This method was developed for distinguishing the signals which were received from scintillator detector with a silicon photomultiplier readout developed for a cosmic ray counter telescope by fitting to pulse shape. The method was verified using experimental data taken in the location $40^{\circ}54'52''$N and $38^{\circ}19'26''$E with the elevation of 30 m above the sea level. The data samples were acquired by the counters which have a scintillator with dimensions of $20\times 20\times 1.4$ cm^3, optically coupled from one side to silicon photomultiplier, then the signals read out by fast sampling digitizer board Domino Ring Sampler board version 4. The method can reconstruct each pulse even for multiple events without losing the count within the small time window. Using this method, 4.969 ns time-of-flight value was established and the rise times for scintillation counters, named Tile 1 and Tile 2, were measured to be about 6.27 ± 0.16 ns and 4.979 ± 0.165 ns, respectively.

DOI:10.5506/APhysPolB.50.1437

1. Introduction

Precisely measuring the timing information of a particle in an experiment would allow one to successfully reconstruct physical events. Time-of-Flight (TOF) methods have been developed and used in many fields such as high-energy physics experiments [1, 2], astroparticle detectors [3, 4], TOF cameras [5, 6], TOF-PET detectors [7, 8] for identifying the particle species, determining the direction of the particles and energy measurements. The counter telescope is useful in research where a relatively few number of desired particles has to be counted in a major unwanted background. To analyze the coincidence time, passing through the counters telescopes, it is practical to remove the spurious counts registered because of the accidental coincidence of counts in each detector. While comparing the Silicon PhotoMultipliers (SiPMs) with traditional PhotoMultiplier Tubes (PMTs), which have been for decades widely used in the past experiments, SiPMs have some advantages such as advanced photon detection efficiency, compactness, excellent single-photon time resolution, insensitivity to magnetic fields and low price. Due to these advantages, they are used in a wide range of physics experiments nowadays. An SiPM signal is constituted of a few different avalanche events formed at arbitrary times. The difficulties in achieving high accuracy on the time-marking of the signal and TOF resolutions of a counter telescope with existing algorithms consist the following subjects:

— *Variation of the baseline:* If the dark count rate increases considerably, then peaks of the signal are mostly overlying on each other within a time latency. Therefore, the method requires to detecting and evaluating the signal starting time for different heights while working at higher over-voltages.

— *Electrical noise:* The signal-to-noise ratio needs to be at the lowest point 5 in the worst conditions (minimum over-voltages and higher electronic noise). If the primary signals will be evaluated which mostly yields an ambiguity of 20% on the signal size while computing directly thus, a fitting algorithm is required.

— *Very different signal heights and widths:* Since the proposed method can be able to adjust itself while measuring various properties without a user concerning to change and optimize the parameters for any evaluation, very different signal heights and widths vary strongly with over-voltage and SiPM [9].

The rest of the paper is organized as follows. In the next section, an experimental setup used for signal reconstruction is described. In Section 3, a method developed to extract time information of the signal coming from scintillation counters without varying difficulties listed above is presented. Finally, an application of this method to the experimental data is constructed and the results are given.

2. Experimental details

2.1. Description of the setup

The hardware of the scintillation counter telescope constructed with two identical scintillator plates, called Tile 1 and Tile 2, set in a distance of 160 cm as seen in figure 1. Each counter box consists of a KURARAY organic scintillator plate ($20 \times 20 \times 1.4$ cm^3). The scintillator has excellent properties, such as yielding the light in blue region of the spectrum and the emission peak around 430 nm which are crucial to get the accurate timing information. Each scintillator panel is wrapped in Tyvek paper for diffusing the reflection, and one SensL SiPM (3×3 mm^2) is contacted to read the produced signal. This SiPM is able to produce a sharp output pulse of < 2 ns at Full Width at Half Maximum (FWHM). The bias voltage of this device is about 27.5 V and the dynamic range over the breakdown voltage is about 2 V. Hence, the filling factor of the device is 64%, the gain is 2.3×10^6 [11]. The produced signal is digitized by the Domino Ring Sampler board (DRS4), developed by Ritt [12]. The Data Acquisition (DAQ) program is based on the setup schematically shown in figure 1. It is managed by a shell script that controls the two main C++ programs. One of the program is controlling the Arduino so that it reads temperatures from the SiPM readout circuit and adjusts the operating voltage in order to keep the gain of the SiPM constant on each tile. The other program manages the Domino Ring Sampler board $v4$ which digitizes the signal detected by the SiPM and stores it in ROOT binary format for further analysis. The DAQ is based on waveform sampling at 2 GS/s, covering a 2.5 μs window. This detector can be used to select horizontal tracks for detecting tau shower produced by the neutrino interacting in Earth crust [13–15]. Thus, the TOF resolution of the selected tracks can be achieved to 0.5 ns.

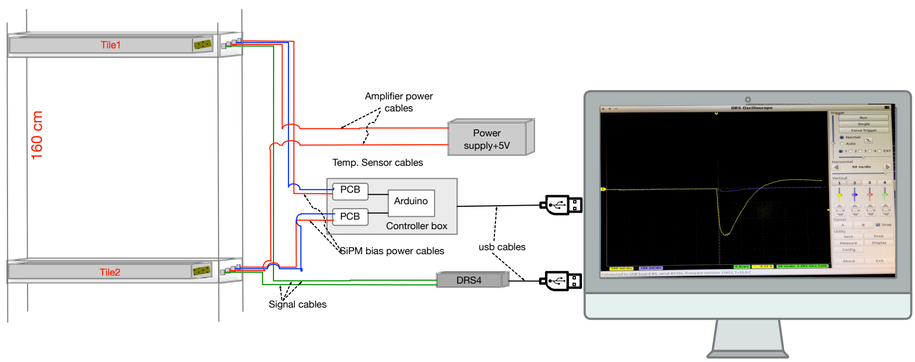

Fig. 1. Schematic view of data acquisition.

2.2. Description of the reconstruction method

The reconstruction program, based on ROOT analysis package [16] using C++ programming language, represents a necessary tool for the analysis of the data. The method is optimized for high sensitivity, while determining the peak level and rise time of the signal are required to effectively use the peak height readout option. The method explained in this section is developed to work on a continuous SiPM signal.

2.2.1. Least square method

A function was written in the analysis program in order to determine the starting point of the signal. This point gives the timing information of the particle so that a mathematical procedure can be applied for estimating the best-fitting curve to a dedicated set of points by minimizing the sum of squares of the offsets (the residuals) from the curve. By substituting a set of N-data points (x_i, y_i) to a straight-line function, we obtain

$$y(x) = mx + c\,, \tag{1}$$

where $y(x)$ and x are holding the voltage and time informations of the SiPM signal, respectively. The equation is generally called *least square method* or *linear regression* [17]. Assuming that the uncertainty σ_i associated with each measurement y_i is known, and the x_is (values of the dependent variable) are known exactly, the chi-square, χ^2, function is used to compute how well the model matches up with the data

$$\chi^2(m, c) = \sum_{i=0}^{N-1} \left[\frac{y_i - mx_i - c}{\sigma_i}\right]^2 . \tag{2}$$

When the errors of a measurement are spread out normally, then this function will yield maximum likelihood coefficient evaluations of m and c; if they are not spread out normally, then the evaluations are not maximum likelihood but might be advantageous to use in a practical sense. In order to determine m and c, Eq. (2) is minimized. At its minimum, derivatives of $\chi^2(m, c)$ with respect to m, c become zero

$$\begin{aligned}\frac{\partial\chi^2}{\partial c} &= -2\sum_{i=0}^{N-1} \frac{y_i - mx_i - c}{\sigma_i^2} = 0\,,\\ \frac{\partial\chi^2}{\partial m} &= -2\sum_{i=0}^{N-1} \frac{x_i(y_i - mx_i - c)}{\sigma_i^2} = 0\,.\end{aligned} \tag{3}$$

These conditions can be revised in a suitable form given in the following sums:

$$\begin{aligned}\xi_\sigma &\cong \sum_{i=0}^{N-1} \frac{1}{\sigma_i^2}\,, \qquad \xi_x \cong \sum_{i=0}^{N-1} \frac{x_i}{\sigma_i^2}\,, \qquad \xi_y \cong \sum_{i=0}^{N-1} \frac{y_i}{\sigma_i^2}\,,\\ \xi_{xx} &\cong \sum_{i=0}^{N-1} \frac{x_i^2}{\sigma_i^2}\,, \qquad \xi_{xy} \cong \sum_{i=0}^{N-1} \frac{x_i y_i}{\sigma_i^2}\,.\end{aligned} \tag{4}$$

Equation (3) can be rewritten by using the definitions in Eqs. (4)

$$\begin{aligned} m\xi_x + c\xi_\sigma &= \xi_y\,, \\ m\xi_{xx} + c\xi_x &= \xi_{xy}\,. \end{aligned} \tag{5}$$

The result of these two equations with two unknowns is computed as

$$\begin{aligned} \varDelta &\cong \xi_\sigma \xi_{xx} - (\xi_x)^2\,, \\ c &= \frac{\xi_{xx}\xi_y - \xi_x\xi_{xy}}{\varDelta}\,, \qquad m = \frac{\xi_\sigma\xi_{xy} - \xi_x\xi_y}{\varDelta}\,. \end{aligned} \tag{6}$$

The solution for the best-fit model parameters m and c is given in Eq. (6). The expected uncertainties in the calculation of m and c should also be evaluated because the measurement errors in the data naturally bring some uncertainty in the setting of those parameters. Assuming the data set is independent, each value puts its own bit of uncertainty to the parameters. Taking into account the spread of errors indicates that the variance σ_f^2 in the value of any function is as follows:

$$\sigma_f^2 = \sum_{i=0}^{N-1} \sigma_i^2 \left(\frac{\partial f}{\partial y_i}\right)^2 . \tag{7}$$

The derivatives of m and c in respect to y_i might be directly calculated from the solution for the straight line equation

$$\frac{\partial c}{\partial y_i} = \frac{\xi_{xx} - \xi_x \xi_{x_i}}{\sigma_i^2 \varDelta}\,, \qquad \frac{\partial b}{\partial y_i} = \frac{\xi_\sigma \xi_x - \xi_{x_i}}{\sigma_i^2 \varDelta} \tag{8}$$

after the summation over the points as in Eq. (7)

$$\sigma_c^2 = \frac{\xi_{xx}}{\varDelta}\,, \qquad \sigma_m^2 = \frac{\xi_{xx}}{\varDelta} \tag{9}$$

which are called the variances in the estimates of m and c, respectively [18, 19].

3. Results

3.1. Application of the Time-of-Flight method to the experimental data

The counter telescope is useful in researches where a relatively a few number of desired particles have to be counted in a major unwanted background. Analyzing the coincidence time is an efficient way of removing the spurious counts occurred due to the accidental coincidence in each detector.

TOF is a method of measuring the time that it takes for a particle to travel a distance in a medium. A particle hitting one of the scintillator tile, as shown in figure 2, starts the time counter which will be stopped when the particle hits the second scintillator tile.

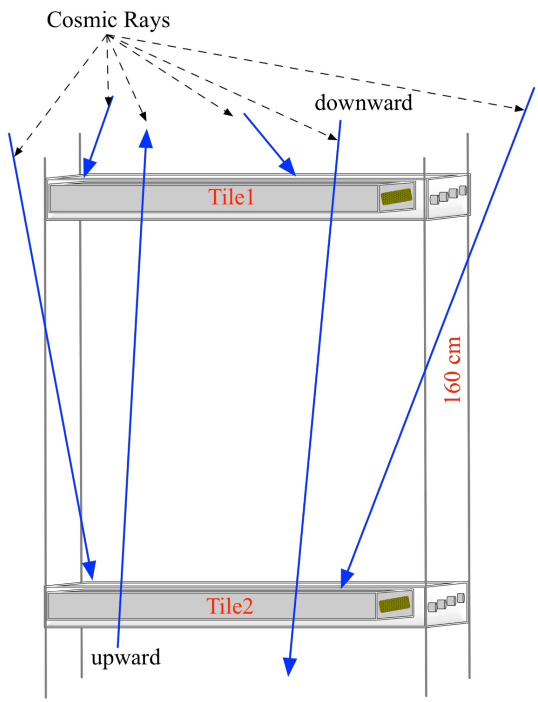

Fig. 2. Schematic view of a counter telescope.

TOF method is also useful to discriminate the particle direction (*upward* or *downward*). Firstly, if the particle hits the Tile 1, then hits the Tile 2, it means the particle is going *downward* direction, the expected result of the time difference ($t_0ch2 - t_0ch1$) should be *positive*, if not, the particle is going *upward* direction.

Figure 3 shows the algorithm used for calculating the Time-Of-Flight method which has been mentioned in Section 2.2.1. The signals are registered by using the DRS4 board and then plotted by ROOT program to observe the time difference between two tiles. If the signal is greater than the threshold voltage (~ 40 mV), then the program estimates the baseline of each signal in order to be insensitive to the baseline instability. After that, if the signal is inside the gate (180 ns–250 ns), the analyzing program firstly finds if the peak level (absolute minimum) of the signal is the 100% of the amplitude, then goes backward until it reaches the *safePoint* (which is at

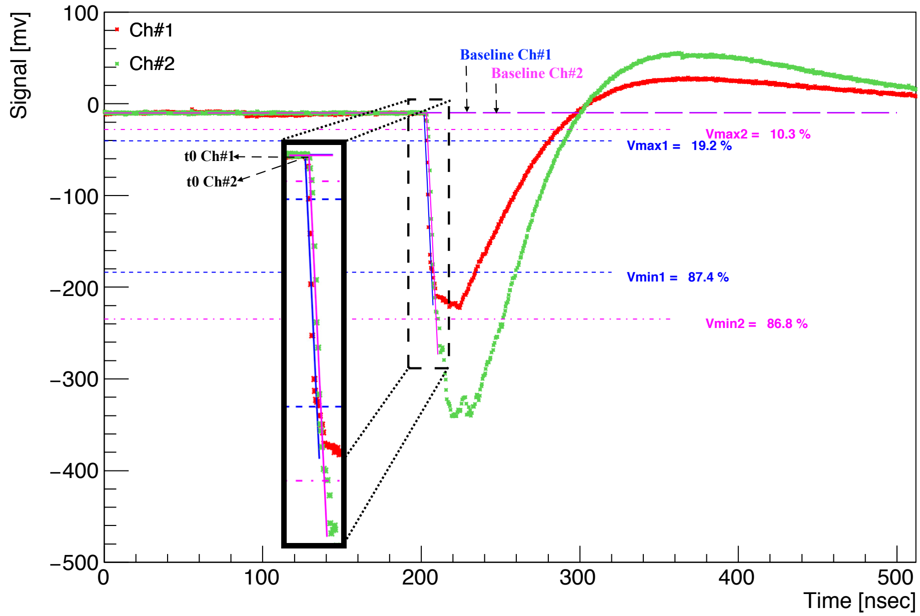

Fig. 3. (Colour on-line) Schematic description of the proposed TOF calculation method used in this study. Magenta and blue lines indicate the fitted results according to the method working forward direction from 10% until 90% of the amplitude of each signal.

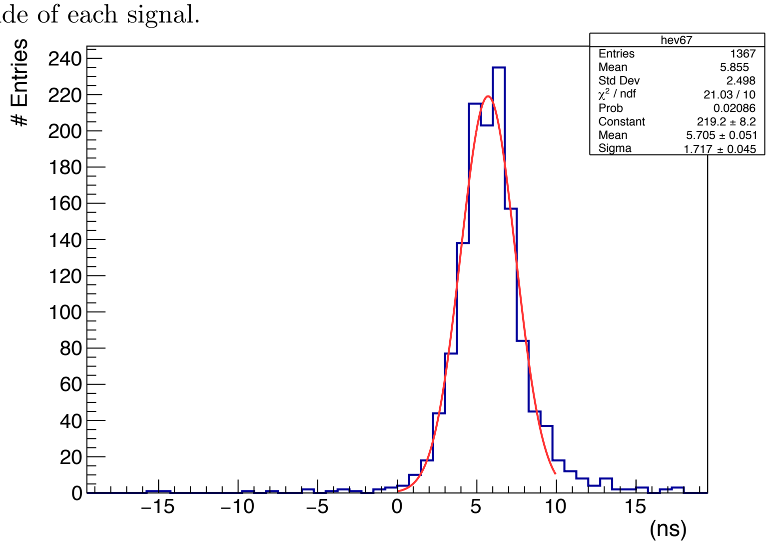

Fig. 4. Time-of-Flight distribution of the counter telescope for tile separation is 160 cm. The peak around +5 ns is due to the particle coming from Tile 1 to Tile 2 (downward direction).

least 3σ below the baseline). Next, the program stores those points for being used in a fit method. The program marks 10% and 90% of the amplitude, which are not fixed number of points, to be just below the threshold value and estimated *safePoint*. The program fits a line equation using these registered points employing the method explained in Section 2.2.1, and crosses its own baseline axis (time axis). This point is registered as t_0. The difference of t_0 gives us the time of flight between two counters.

Figure 3 shows the scheme of this algorithm. The computed TOF is about 5 ± 1.7 ns for a *downward* going particle as shown in figure 4.

3.2. Rise time test

Time taken by the signal to rise from minimum level to maximum level is named the *rise time*, and the time taken by the signal that goes from maximum level to minimum level is named *fall time*. The nonlinearity of the signal typically takes place at the bottom and at the top of the signal so that the rise time is generally determined between the 10% and 90% of the amplitude of the signal. A typical SiPM signal registered by the detector is seen in figure 5. It has a final rise and fall times. The results are given in figure 6.

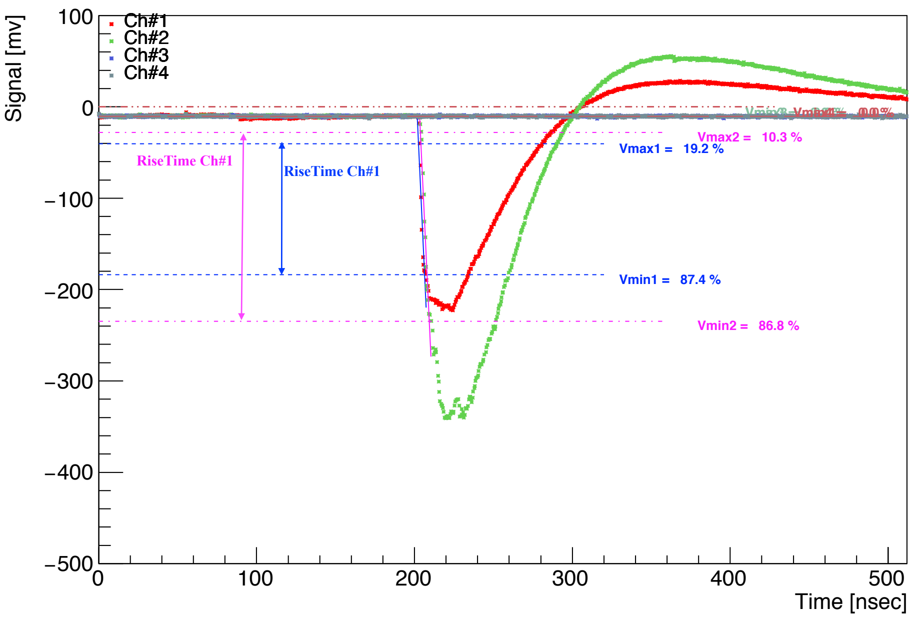

Fig. 5. Signal shape of the rising time between the boundaries of 10% and 90% of the amplitude.

In figure 6, the mean values of the Gaussian fit on the rising time distribution are 6.27 ± 0.16 ns and 4.979 ± 0.165 ns for Tile 1 and Tile 2, respectively.

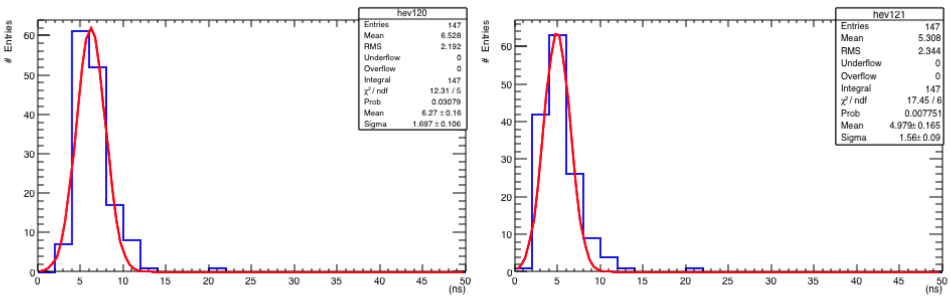

(a) Tile 1 (b) Tile 2

Fig. 6. Rising time distribution of the signal is between 10% and 90% of the amplitude. (a) is for Tile 1 and in (b) is for Tile 2.

3.2.1. Testing the robustness of the fit

Goodness of fit, R^2, called correlation coefficient, is a quantity which indicates the quality of a least square fitting to the data. If $R^2 = 1$, it means the fit is perfect but it is generally expected that it is close to 1. Figure 7 depicts the R^2 distribution for all registered events for each tile. The mean values are 0.9752 and 0.9654 for Tile 1 and Tile 2, respectively.

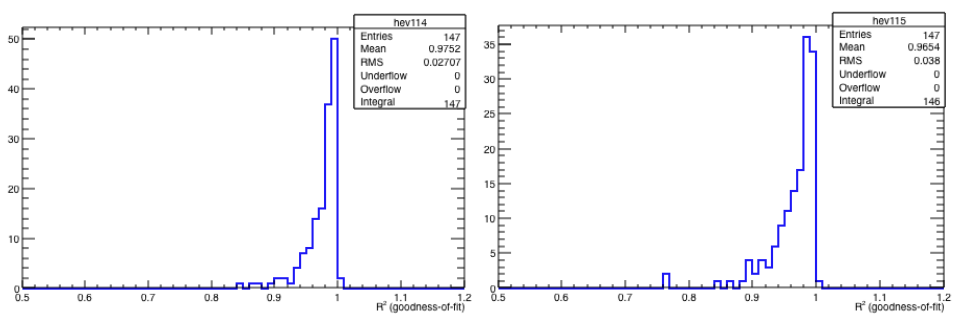

(a) Tile 1 (b) Tile 2

Fig. 7. Goodness of fit distribution of the signal is between 10% and 90% of the amplitude. (a) is for Tile 1 and in (b) is for Tile 2.

3.3. *Multiplicity of the signal test*

The signal (seen in figure 3) is a single cosmic ray (generally muon) pointing towards the region of the SiPMs. Cosmic rays are large collections of particles. Since these cosmic rays contain many particles, the particles will often separate, which could cause multiple hits in the region of the SiPM. One can see that there are two main hits in the given particular event (seen in figure 8).

Multiplicity is defined as a number of hits per event inside the full sampling window of the SiPMs which is sketched in figure 8. Since the detector is not limited to one characteristic of event, the both particles would be present, and point towards a nearby region, causing the total charge to be excessed.

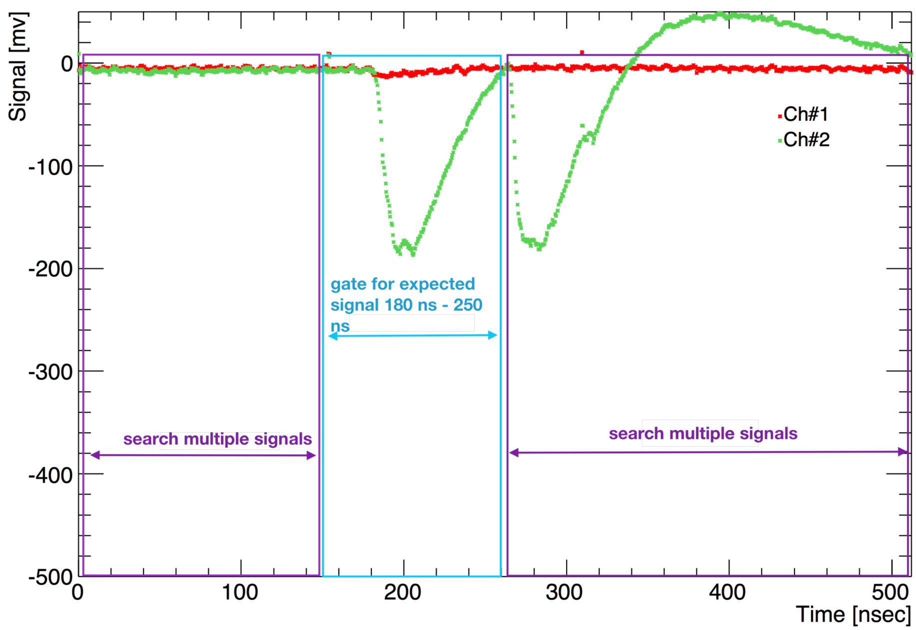

Fig. 8. Multiplicity of registered SiPM signal in a full sampling window.

In order to find the multiplicity of the signals, the total charge of the expected signal in the window gate (180 ns–250 ns) and the total charge of the all signals in the full sampling window (512 ns) were integrated, and the baseline of each signal was removed from the total charge. Figure 9 shows the integrated charge for the signals in the full sampling window ((a) Tile 1 and (b) Tile 2) and the signals within the gated window ((c) Tile 1 and (d) Tile 2).

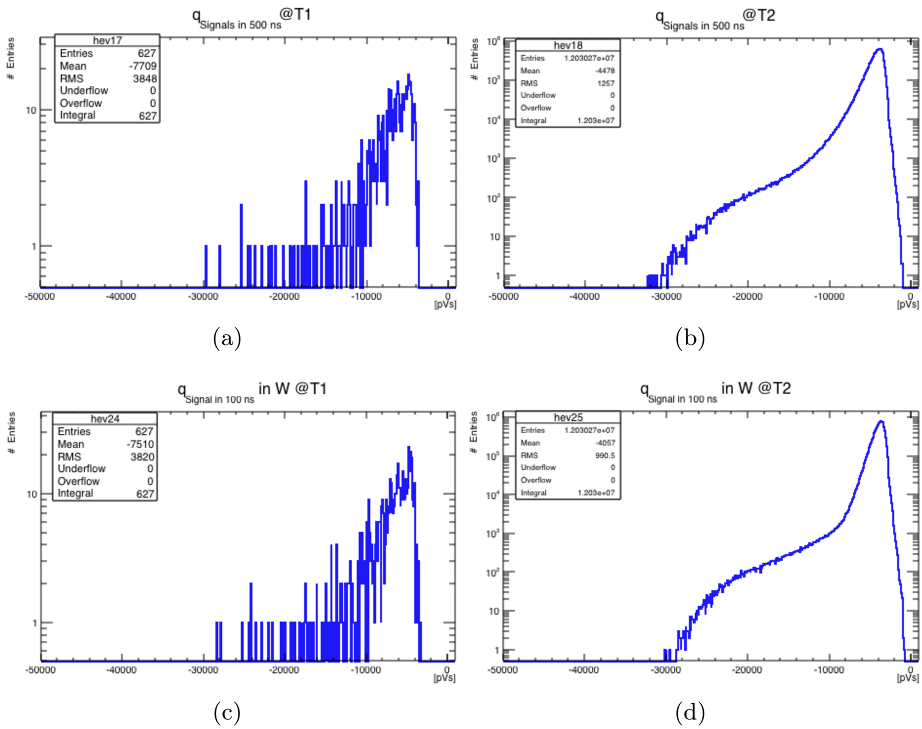

Fig. 9. Integrated charge for all signals where the baseline was removed from each signal. Histograms depict that the excessive number of particles in (a) is for Tile 1 and in (b) is for Tile 2. The integrated charge for gated signals in (c) is for Tile 1 and in (d) is for Tile 2. DAQ trigger channel is Tile 2.

Figure 10 ((a) Tile 1, (b) Tile 2), depicts the multiplicity as a function of the integrated charge which was estimated by subtracting the total charge of the signal in the defined region from the total charge of the signals in the full sampling window. The multiplicity number as a function of the expected signal was also estimated and plotted in figure 10 ((c) Tile 1, (d) Tile 2). The values above 1 are due to more than one particle interacting with one cell. Since Tile 2 was selected as a trigger in the DAQ, the number of registered signals was statistically higher than Tile 1 as shown in figures 9 and 10.

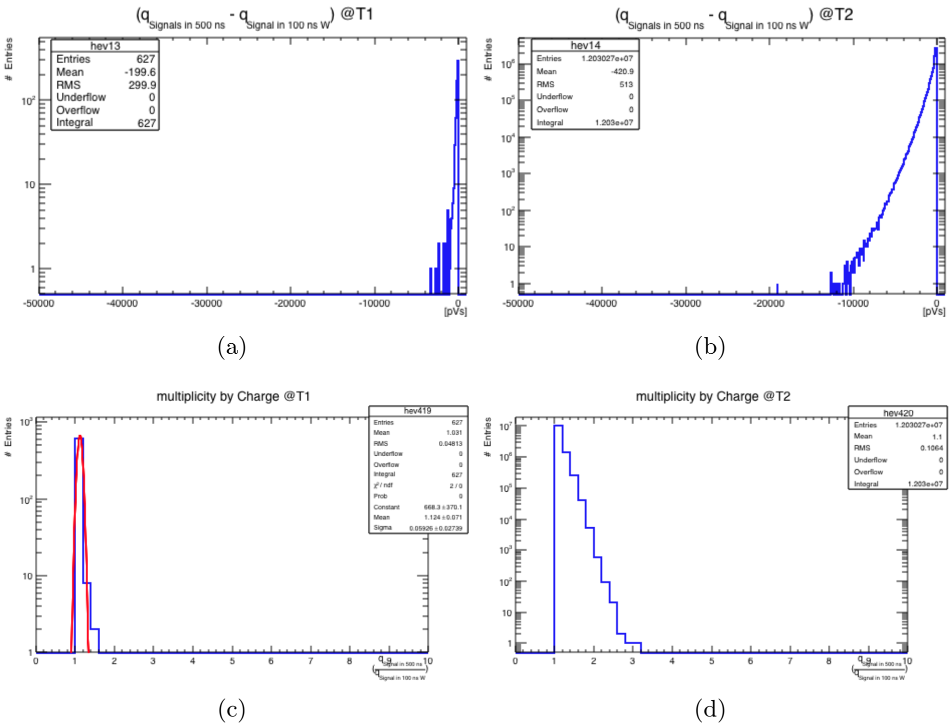

Fig. 10. Multiplicity events in terms of integrated charge for the full sampling window (a) for Tile 1 and (b) for Tile 2, and (c) and (d) give the multiplicity in terms of the number of events. DAQ trigger channel is Tile 2.

4. Discussion and conclusion

In this paper, the performance study of the developed method for time-of-flight measurements using the scintillation counters are presented. A new DAQ system, described in Section 2.1, is working automatically without any interaction of a user. Moreover, a new program and a time-of-flight technique were developed and tested for further analysis. The rise time of the SiPM signals was accumulated and found to be 6.27 ± 0.16 and 4.979 ± 0.165 ns for each tile. The coincidence timing resolution between the tiles was found to be about 1.7 ns signal (see figure 4). Multiplicity as a function of the integrated charge of the signals was estimated around -119.6 pVs (-420 pVs) for Tile 1 (Tile 2). The limitation on the results is due to the present electronics used in the DAQ system. These results prove that using of this developed method satisfies very well the selection of direction of cosmic rays while removing the background.

I would like to thank Prof. Dr. Haluk Denizli and Prof. Dr. Maurizio Iori for their support and encouragement during the course of this work.

REFERENCES

[1] S. Barwick *et al.*, *Nucl. Instrum. Methods Phys. Res. A* **400**, 34 (1997).
[2] A. Alici, *Nucl. Instrum. Methods Phys. Res. A* **766**, 288 (2014).
[3] B.N. Ratcliff, *Nucl. Instrum. Methods Phys. Res. A* **595**, 1 (2008).
[4] M. Iori *et al.*, *Nucl. Instrum. Methods Phys. Res. A* **742**, 265 (2014).
[5] F. Mufti, R. Mahony, *ISPRS J. Photogramm. Remote Sens.* **66**, 720 (2011).
[6] M. Gilles *et al.*, *Radiother. Oncol.* **115**, S823 (2015).
[7] A. Ronzhin *et al.*, *Nucl. Instrum. Methods Phys. Res. A* **703**, 109 (2013).
[8] C. Joram, *Nucl. Instrum. Methods Phys. Res. A* **732**, 586 (2013).
[9] M. Putignano, A. Intermite, C. Welsch, *JINST* **7**, P08014 (2012).
[10] `http://kuraraypsf.jp/psf/`
[11] `https://www.sensl.com/`
[12] S. Ritt, *Nucl. Instrum. Methods Phys. Res. A* **518**, 470 (2004).
[13] M. Iori, A. Sergi, D. Fargion, `arXiv:astro-ph/0409159`.
[14] M. Iori, A. Sergi, *Nucl. Instrum. Methods Phys. Res. A* **588**, 151 (2008).
[15] A. Yilmaz *et al.*, *PoS* **ICRC2017**, 471 (2018).
[16] R. Brun, F. Rademakers, *Nucl. Instrum. Methods Phys. Res. A* **389**, 81 (1997).
[17] S. Margulies, *Rev. Sci. Instrum.* **39**, 478 (1968).
[18] W.H. Press, S.A. Teukolsky, B.P. Flannery, W.T. Vetterling, *Numerical Recipices, The Art of Scientific Computing*, 3$^{\rm rd}$ edition, Cambridge University Press, 2007.
[19] E.W. Weisstein, *Least Squares Fitting*, from: MathWorld — A Wolfram Web Resource, `http://mathworld.wolfram.com/LeastSquaresFitting.html`